Role of Arginine 138 in the Catalysis and Regulation of *Escherichia coli* Dihydrodipicolinate Synthase†

Renwick C. J. Dobson,*,‡ Sean R. A. Devenish,‡ Leighton A. Turner,‡ Veronica R. Clifford,‡ F. Grant Pearce,‡ Geoffrey B. Jameson,§ and Juliet A. Gerrard*,‡

School of Biological Sciences, University of Canterbury, Private Bag 4800, Christchurch, New Zealand, and Centre for Structural Biology, Institute of Fundamental Sciences, Massey University, Palmerston North, New Zealand

Received July 4, 2005; Revised Manuscript Received July 26, 2005

ABSTRACT: In plants and bacteria, the branch point of (*S*)-lysine biosynthesis is the condensation of (*S*)-aspartate-β-semialdehyde [(*S*)-ASA] and pyruvate, a reaction catalyzed by dihydrodipicolinate synthase (DHDPS, EC 4.2.1.52). It has been proposed that Arg138, a residue situated at the entrance to the active site of DHDPS, is responsible for binding the carboxyl of (*S*)-ASA and may additionally be involved in the mechanism of (*S*)-lysine inhibition. This study tests these assertions by mutation of Arg138 to both histidine and alanine. Following purification, DHDPS-R138H and DHDPS-R138A each showed severely compromised activity (approximately 0.1% that of the wild type), and the apparent Michaelis−Menten constant for (*S*)-ASA in each mutant, calculated using a pseudo-single substrate analysis, was significantly higher than that of the wild type. This provides good evidence that Arg138 is indeed essential for catalysis and plays a key role in substrate binding. To test whether structural changes could account for the change in kinetic behavior, the solution structure was probed via far-UV circular dichroism, confirming that the mutations at position 138 did not modify secondary structure. The crystal structures of both mutant enzymes were determined, confirming the presence of the mutations and suggesting that Arg138 plays an important role in catalysis: the stabilization of the catalytic triad residues, a motif we have previously demonstrated to be essential for activity. In addition, the role of Arg138 in (*S*)-lysine inhibition was examined. Both mutant enzymes showed the same IC_{50} values as the wild type but different partial inhibition patterns, from which it is concluded that arginine 138 is not essential for (*S*)-lysine inhibition.

Dihydrodipicolinate synthase (DHDPS,[1] EC 4.2.1.52) is the enzyme that catalyzes the branch point reaction leading to *meso*-diaminopimelate (DAP) and (*S*)-lysine. First characterized in 1965 (*1*), DHDPS has since attracted sustained interest in the literature. (*S*)-Lysine biosynthesis occurs in plants and microorganisms, but not in animals, and thus draws continued attention as a target for antibiotics and herbicides (*2*, *3*), although no potent inhibitor of DHDPS has yet been found. As the purported rate-determining step in (*S*)-lysine biosynthesis, DHDPS is of interest to biotechnologists aiming to engineer crops rich in (*S*)-lysine, often the limiting nutrient in staple crops (*4*).

DHDPS catalyzes the condensation of (*S*)-aspartate-β-semialdehyde [(*S*)-ASA] and pyruvate. The product is likely to be an unstable heterocyclic product, now thought to be (4*S*)-4-hydroxy-2,3,4,5-tetrahydro-(2*S*)-dipicolinic acid (HTPA). The currently accepted mechanism of DHDPS is outlined in Figure 1, in which the structure of (*S*)-ASA is presumed to be the hydrate (*5*). In the first step of the mechanism, the active site lysine residue (Lys161 in *Escherichia coli*) forms a Schiff base with pyruvate, as has been proposed in several studies (*6*−*8*). Subsequent binding of (*S*)-ASA, the second substrate in the reaction, is followed by dehydration and then cyclization to form the product, which is released into solution. On the basis of the X-ray crystal structure of the *E. coli* enzyme (*5*, *9*), sequence homologies with DHDPS from other sources (*10*), and our own mutagenic studies (*11*), it is proposed that a catalytic triad of three residues, Tyr133 and Thr44 from one subunit and Tyr107 from the second subunit in the tight dimer, acts as a proton shuttle to transfer protons to and from the active site.

Arginine 138, which is highly conserved in DHDPS enzymes, sits at the entrance to the active site and, as such, has been implicated in the binding of (*S*)-ASA; Blickling et al. (*5*) showed via X-ray crystallography that the guanidine moiety of Arg138 bound the carboxyl group of succinate semialdehyde, an analogue of (*S*)-ASA. Additionally, Joerger et al. (*12*) have shown that the introduction of an arginine into the equivalent position of *N*-acetylneuraminate lyase from *E. coli* increases DHDPS activity for this enzyme but only marginally increases the affinity for the substrate (*S*)-ASA. They suggest that Arg138 is only partially responsible for substrate binding and may have a hitherto unknown role in catalysis. Interestingly, Guillén Schlippe et al. (*13*) have

† This work was funded by the Royal Society of New Zealand Marsden Fund (Contract UOC303). Funding for the protein X-ray diffraction facility was provided, in part, by The Allan Wilson Centre for Molecular Ecology and Evolution.

* To whom correspondence should be addressed. E-mail: renwick.dobson@canterbury.ac.nz or juliet.gerrard@canterbury.ac.nz.

‡ University of Canterbury.

§ Massey University.

[1] Abbreviations: HTPA, (4*S*)-4-hydroxy-2,3,4,5-tetrahydro-(2*S*)-dipicolinic acid; DHDPS, dihydrodipicolinate synthase; DHDPR, dihydrodipicolinate reductase; (*S*)-ASA, (*S*)-aspartate-β-semialdehyde; DAP, *meso*-diaminopicolinate.

10.1021/bi051281w CCC: $30.25
Published on Web 09/02/2005

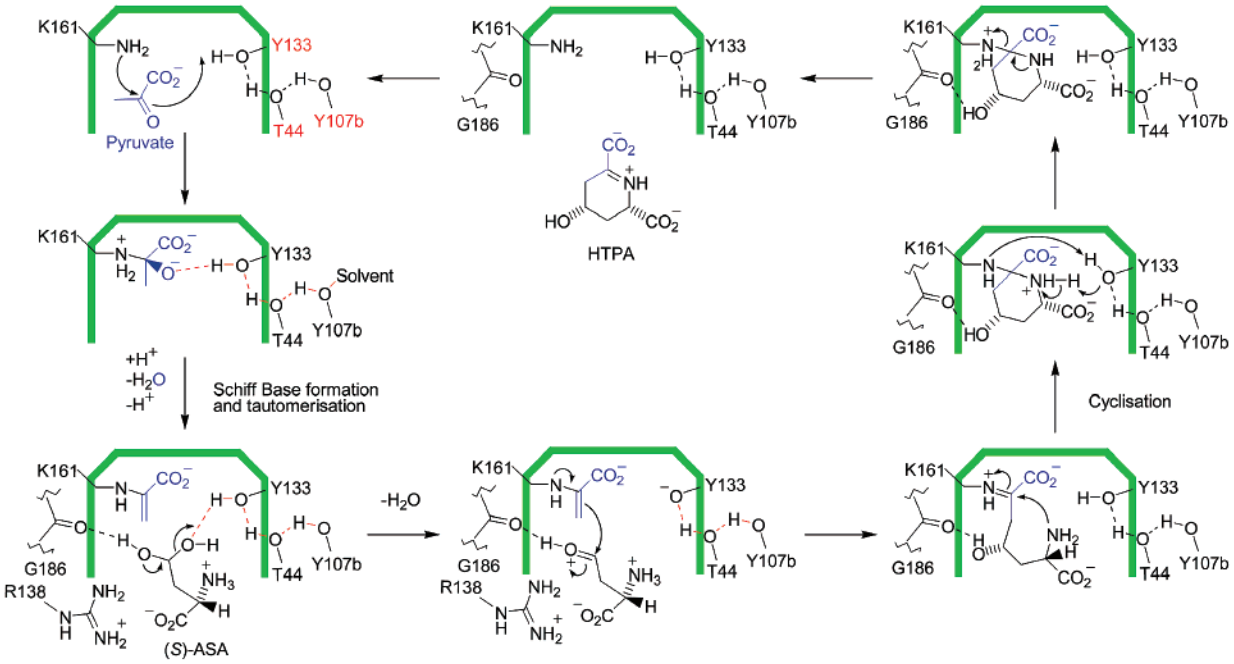

FIGURE 1: Putative roles for the catalytic triad in the mechanism of DHDPS. This mechanism has been adapted from Hutton et al. (*3*). In this mechanism, Tyr133 is proposed to act both as a general acid and as a general base. Y107b signifies that tyrosine 107 is supplied to the active site by subunit B in the tight dimer of DHDPS.

shown that arginine residues, if solvent accessible and adjacent to a carboxyl moiety, are capable of exhibiting unusually low pK_a values and thus able to act as a general base during catalysis. Arg138 satisfies these requirements when interacting with (*S*)-ASA.

Catalyzing the branch point reaction in (*S*)-lysine biosynthesis, DHDPS is a key regulatory point. (*S*)-Lysine binds DHDPS to partially attenuate catalytic activity. Blickling et al. (*5*) assert that the binding of free (*S*)-lysine to the allosteric binding site causes inhibition of enzyme activity by increasing the rigidity of Arg138. Our studies have found, however, that (*S*)-lysine binding causes the opposite affect (*14*). The mechanisms of (*S*)-lysine inhibition, and the role of Arg138 in such mechanisms, are not understood.

In an effort to resolve these issues, we embarked upon mutagenic and subsequent structural studies of DHDPS, here focusing in particular on Arg138. Two mutations were studied: Arg138His, which retained some of the steric bulk and potential general base activity of an arginine, but was unlikely to interact with the carboxyl of (*S*)-ASA in the same way, and Arg138Ala, which potentially removed all side chain functionality at this position.

MATERIALS AND METHODS

Materials. Unless otherwise stated, all chemicals were obtained from Sigma Chemical Co. or Amersham Biotechnologies. Protein concentration was measured by the method of Bradford (*15*). Enzymes were manipulated at 4 °C, or on ice, and were stored in Tris-HCl buffer (20 mM, pH 8) at −20 °C. (*S*)-ASA was synthesized using the methods of Roberts et al. (*16*) and was of the highest quality (>95%) as judged by ^{1}H NMR and the coupled assay. Stock solutions of (*S*)-ASA and NADPH were prepared fresh for each experiment. Dihydrodipicolinate reductase (DHDPR), required for the coupled assay, was purified by previously reported methods (*11*).

Site-Directed Mutagenesis. Alterations in *dapA* (the *E. coli* gene for DHDPS cloned into a pBluescript vector) were introduced using the Quikchange site-directed mutagenesis kit (Stratagene). The parent plasmid was pJG001 (*2*). The reaction conditions followed the manufacturer's instructions, except that the annealing temperature in the PCR reaction was lowered to 50 °C. Successful mutation was judged by an altered restriction pattern when cut with *Rsa*1, and confirmation was afforded by sequencing using the T7 and T3 priming sites, which was performed at the University of Auckland Sequencing Facility.

Overexpression and Purification. Mutant forms of the enzyme were expressed in *E. coli* AT997r− (*11*). The purification methods of Dobson et al. (*11*) were followed for each mutant DHDPS form.

Far-Ultraviolet Circular Dichroism (CD). CD spectra (Olis DSM-10) were recorded at 0.5 or 2 nm intervals over the 185−250 nm wavelength range using a 1 mm path length quartz cell. The reported spectra were the average of four scans that were smoothed and corrected for buffer blanks. The temperature was maintained at 20 °C. The buffer used for CD measurements was 20 mM Na_2HPO_4/150 mM NaF (pH 8), against which the protein solutions (~8 μM) were dialyzed. Measured CD traces (CD_{meas}) were converted to mean residue ellipticity [Θ] (deg cm^2 dmol $^{-1}$) using the relationship $[\Theta] = CD_{meas}$ (mdeg) $\times$ 100/[C (mM) l (cm) NR], where NR is the number of residues per peptide, l the cell length, and C the protein concentration (determined using the A_{280}, $\epsilon = 12690$ M^{-1} cm^{-1}).

Kinetics. DHDPS activity was measured using a coupled assay with DHDPR, as previously described (*2*), with the following modifications. The low activity of the mutants

necessitated the addition of greater quantities of enzyme to the assay. The reaction was therefore initiated with (*S*)-ASA after the cuvette had been preincubated for 10 min. Assays were performed in HEPES buffer (100 mM, pH 8) at 30 °C, kept constant using a circulating water bath. Care was taken to ensure that the enzymes and substrates were stable over the course of the assay (usually 2 min). The stability of the mutants under the conditions of the assay was examined using Selwyn's test (*17*) and was found to be constant (data not shown). Care was also taken to ensure an excess of DHDPR; about 20 μg per assay was used. The amount of enzyme added to each assay depended on the activity of the individual mutants; however, it was ensured that enzyme concentration was proportional to initial rate. Initial velocities were usually reproducible within 10% error.

Initial rate data were analyzed using the Enzfitter program available from Biosoft (Cambridge, U.K.) and were fitted to the Michaelis−Menten kinetic model:

$$\upsilon = VA/(K_m^{app} + A) \quad (1)$$

Here V is the maximal velocity, A is the substrate concentration, K_m^{app} is the apparent Michaelis−Menten constant, and υ is the initial velocity (*18*). Initial kinetic trials for the mutants indicated the K_m^{app} for (*S*)-ASA had substantially increased, necessitating the curmudgeonly use of this substrate. Thus, using pseudo-single substrate kinetics, apparent kinetic parameters were obtained. For the same reasons, and because of the lower initial rates, when testing the mutants versus (*S*)-lysine inhibition, approximate IC_{50} values were obtained.

Crystallization and X-ray Data Collection. The crystallization experiments were undertaken as described by Mirwaldt et al. (*9*) using the hanging drop−vapor diffusion method at 12 °C. Each drop contained protein solution (~5 mg/mL in Tris-HCl, 20 mM, pH 8, 2.5 μL), precipitant (K_2HPO_4, 1.8 M, pH 10, 1.2 μL), and *N*-octyl-β-*R*-glucopyranoside (6% w/v, 0.6 μL). Crystals appeared after 3−5 days and grew to dimensions of up to 0.4 mm. For X-ray data collection, the crystals were soaked in cryoprotectant solution [K_2HPO_4, 2.0 M, pH 10, 20% glycerol (v/v)] and directly flash-frozen in liquid nitrogen. Intensity data were collected at 110 K using an RAxisIV++ image-plate detector coupled to a Rigaku Micromax 007 X-ray generator operating at 40 kV and 20 mA. The crystals belong to space group $P3_121$ and diffracted to beyond 2.05 Å resolution. Diffraction data sets were processed and scaled using the package CrystalClear (*19*).

Structure Determination and Refinement. The orientation and location of each DHDPS mutant structure were determined using molecular replacement [AMoRe (*20*)], where the search model was the *E. coli* DHDPS monomer (PDB code 1YXC) with position 138 initially annotated as a glycine. The asymmetric unit contained two monomers, which together made up the tight dimer. Refinement was achieved using Refmac5 (*21*) with manual model corrections using the program O (*22*). The final refinement rounds involved the placement of solvent molecules using the program Arp (*23*). Dataman was used to transfer the R_{free} flags from the wild-type data set to the mutant data sets. Procheck (*24*) was used to examine the quality of the final structures. In both mutant structures, 94.5% of the residues (within the asymmetric unit) fell into the most favored regions of the Ramachandran plot, 5.1% in the generously allowed region, and 0.4% in the disallowed region. Data collection and model refinement statistics are summarized in Table 1. For each structure, the coordinate and structure factor files were deposited with the RCS Protein Data Bank (DHDPS-R138A, 2A6N; DHDPS-R138H, 2A6L). Images in this work were produced with Pymol (*25*).

Table 1: Data Collection and Refinement Statistics[a]

	DHDPS-R138A	DHDPS-R138H
resolution (data processing, Å)	1.80 (1.86−1.80)	2.05 (2.12−2.05)
no. of images	318	235
oscillation range (deg)	0.3	0.3
space group	$P3_121$	$P3_121$
unit cell [*a*, *b*, *c* (Å)]	120.99, 120.99, 111.30	121.02, 121.02, 111.41
no. of reflections/unique	491142/87227	248925/59240
completeness (%)	100.0 (100.0)	99.7 (99.0)
R_{merge}[b] (outer shell)	0.063 (0.394)	0.087 (0.353)
I/σ	14.0 (4.0)	10.4 (3.8)
resolution (refinement, Å)	1.949 (1.991−1.949)	2.05 (2.103−2.05)
R_{free}[c]	0.191 (0.284)	0.212 (0.308)
R_{cryst}[d]	0.163 (0.233)	0.172 (0.248)
mean *B* value (Å^2)	20.6	23.7
estimated coordinate error[e]	0.067	0.096
residues/solvent molecules	584/596	584/550
rmsd from ideal geometry		
bond lengths (Å)	0.011	0.007
bond angles (deg)	1.34	1.11

[a] Values in parentheses represent the highest resolution shell. [b] $R_{merge} = \sum|I - \langle I\rangle|/\sum I$. [c] R_{free} is based on 5% of the total reflections excluded from refinement. [d] $R_{cryst} = \sum||F_o| - |F_c||/\sum|F_o|$. [e] Based on maximum likelihood calculations.

RESULTS AND DISCUSSION

Site-Directed Mutagenesis and Purification. For the site-directed mutagenesis of *dapA*, primers were designed such that successful mutation resulted in a new restriction site, allowing rapid confirmation of successful mutagenesis by inspection of the plasmid's restriction map. Additionally, both plasmids containing a mutated *dapA* gene were sequenced, confirming the presence of the mutation and the integrity of the gene (data not shown).

Transformation of AT997r− with the mutated plasmids provided a convenient method for producing pure samples of the gene product without risk of contamination by wild-type DHDPS (*11*). When transformed, the mutant plasmids rescued AT997r− in the absence of DAP, which suggested that each showed sufficient DHDPS activity for survival. After the cells were lysed by sonication, the cell lysates retained sufficient activity that DHDPS presence could be detected using the *o*-aminobenzaldehyde assay, which facilitated further purification. During purification, all of the mutant forms showed identical heat stability and chromatographic behavior to that of the wild type. When analyzed by SDS−PAGE, each enzyme showed a single band corresponding to the expected monomeric mass of approximately 31000 Da. CD spectra were obtained for both mutant enzymes and compared to the wild-type spectrum in order to examine whether the solution structure had been altered. It can be seen from Figure 2 that all spectra overlaid, confirming structural integrity of both DHDPS-R138A and DHDPS-R138H.

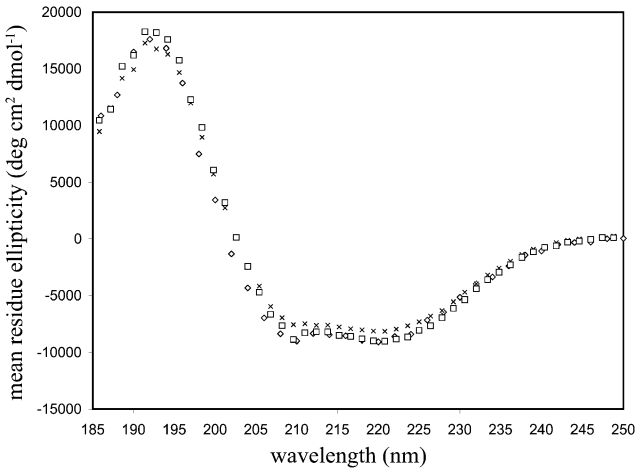

FIGURE 2: UV circular dichroism spectra for the wild-type (◇), DHDPS-R138A (□), and DHDPS-R138H (×).

Crystallization, Refinement, and General Structural Features of the Mutants. Both X-ray crystal structures were determined using the molecular replacement method starting with the wild-type structure available from the Protein Data Bank, entry 1YXC. The final models contained 292 amino acid residues in each chain, with two chains in each asymmetric unit, from which the tetramer can be generated by crystallographic symmetry. The current R_{cryst} and R_{free} values are 16.1% and 19.2% for DHDPS-R138A and 17.2% and 21.2% for DHDPS-R138H. The structures were checked with Procheck (*24*), and all residues, apart from Tyr107 ($\phi \sim 80°$, $\psi \sim -45°$), fell within the allowed regions of the Ramachandran plot (*26*). For position 107, each of the mutant structures showed well-defined electron density, and the dihedral angles were similar to those of the wild-type structure. This residue forms the central residue of a classic γ-turn, as described by Rose et al. (*27*). Others have proposed that the conformational strain at position 107 is consistent with its proposed role in catalysis via the catalytic triad motif (*5*). For both structures, the orientation of the active site residues was the same between both monomers within the asymmetric units (rmsd for monomers in the asymmetric unit were 0.19 Å for DHDPS-R138H and 0.18 Å for DHDPS-R138A).

DHDPS from *E. coli* is a homotetramer (*6*), and the monomer is a $(\beta/\alpha)_8$-barrel with the active site situated within the center of the β-barrel in each monomer (Figure 3). The quaternary structure reveals a dimer of dimers with strong connections between monomers A and B but weak connections between the dimers (*9*, *11*). Neither mutant structure showed any modification in its tertiary or quaternary structures from that of the wild type, a result confirming that gross structural changes were not the cause of the mutated enzymes' attenuated function. Intriguingly, electron density was discovered within the active site of DHDPS-R138H but not DHDPS-R138A. The density was very similar to that seen in the DHDPS-Y107F mutation (*11*) (Figure 4), and its identity is yet to be confirmed. Preliminary results suggest that the tetrahedral intermediate, which is prior to Schiff base formation (as outlined in Figure 1), may fit most of the observed density. However, its occupancy is likely to be less than unity. We can exclude molecules that were added to the crystallization or purification media, suggesting the adduct endured the purification procedure.

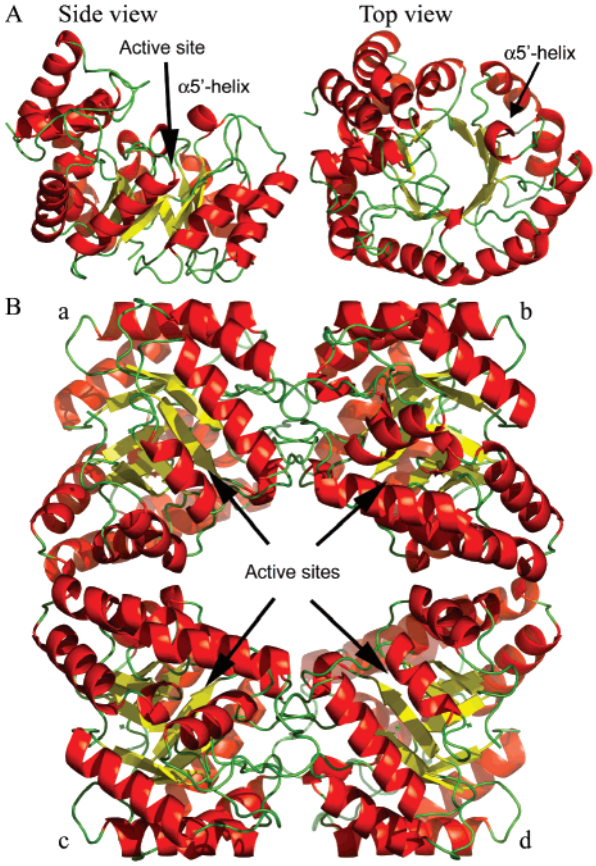

FIGURE 3: Tertiary and quaternary structures of DHDPS-R138A. (A) The monomeric $(\alpha/\beta)_8$-barrel structure of DHDPS-R138A. The α5′-helix, residues 136−139, is highlighted. (B) Quaternary structure of DHDPS-R138A showing the tetramer, which is composed of two tight dimers (a/b and c/d).

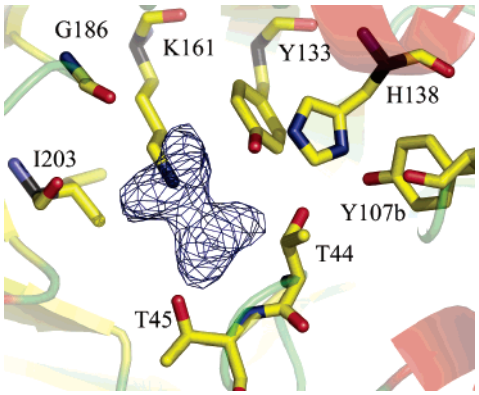

FIGURE 4: Unexplained density ($F_o - F_c$, contoured to 3σ, blue) at the active site of DHDPS-R138H.

Mutant Properties. (a) Kinetics. When comparing the properties of DHDPS-R138A and DHDPS-R138H with the wild type, it was clear that the introduction of an alanine or histidine at this position had a major impact on the catalytic function. Comparing the kinetic properties (Table 2) showed that k_{cat} was decreased by approximately 100−1000-fold, a result similar to other mutations in the DHDPS active site (*11*) and consistent with the hypothesis that arginine 138 is important in catalysis. Not surprisingly, the mutations also altered the ability of the enzyme to bind its substrates. While the K_{mPyr}^{app} (0.45 ± 0.07 mM for DHDPS-R138A and 0.28 ± 0.03 mM for DHDPS-R138H) was only marginally altered compared to the wild type (0.26 ± 0.03 mM), the K_{mASA}^{app}

Table 2: Kinetic Parameters for Wild-Type and Mutant DHDPS Enzymes

wild type[a]			DHDPS-R138A[b]	DHDPS-R138H[c]
k_{cat} (s^{-1})	124 ± 6.8	k_{catPyr}^{app} (s^{-1})	0.149 ± 0.004	0.038 ± 0.001
rel k_{cat} (%)	100		0.1	0.03
		k_{catASA}^{app} (s^{-1})	0.92 ± 0.02	0.17 ± 0.01
rel k_{cat} (%)	100		0.7	0.1
K_{mPyr} (mM)	0.26 ± 0.03	K_{mPyr}^{app} (mM)	0.45 ± 0.07	0.28 ± 0.03
K_{mASA} (mM)	0.11 ± 0.01	K_{mASA}^{app} (mM)	5.1 ± 0.3	37 ± 5
k_{cat}/K_{mPyr} (M^{-1} s^{-1})	$(4.8 \pm 0.6) \times 10^5$	$k_{catPyr}^{app}/K_{mPyr}^{app}$ (M^{-1} s^{-1})	330 ± 10	130 ± 10
k_{cat}/K_{mASA} (M^{-1} s^{-1})	$(1.1 \pm 0.2) \times 10^6$	$k_{catASA}^{app}/K_{mASA}^{app}$ (M^{-1} s^{-1})	180 ± 10	4.0 ± 0.6

[a] From Dobson et al. (*11*). [b] When assaying vs (*S*)-ASA, pyruvate was held constant at 15 mM; when assaying vs pyruvate, (*S*)-ASA was held constant at 3 mM. [c] When assaying vs (*S*)-ASA, pyruvate was held constant at 15 mM; when assaying vs pyruvate, (*S*)-ASA was held constant at 11.3 mM.

values were greatly increased (5.1 ± 0.3 and 37 ± 5 mM for DHDPS-R138A and DHDPS-R138H, respectively) compared to the wild type (0.11 ± 0.01 mM). This is entirely consistent with the role of Arg138 being able to bind the carboxyl moiety of (*S*)-ASA. The unaltered K_{mPyr}^{app} suggests that the guanidinium group of arginine is not involved in binding pyruvate and that the structure and electrostatics of the pyruvate binding pocket remain intact.

That both mutations have similar k_{cat} values and that DHDPS-R138A shows greater affinity for (*S*)-ASA compared to DHDPS-R138H indicate histidine cannot in any way substitute for arginine at this position. We conclude that either Arg138 does not act as a general base or that this is due to the different positioning of the imidazole of histidine compared to the guanidinium of arginine at position 138. The lower K_{mASA}^{app} for DHDPS-R138A, with respect to DHDPS-R138H, suggests that interactions between (*S*)-ASA and the histidine are unfavorable, perhaps due to steric interactions.

(b) Active Site Structures. Following kinetic analysis, protein X-ray crystallography was used to evaluate whether changes in the orientations of residues in the active site could account for the observed kinetic changes. Upon inspection of the initial $F_o - F_c$ difference density map, the alanine and histidine residues at position 138, initially modeled as glycine, were clearly visible (Figure 5). Arginine 138 is situated on the short α5′-helix [as denoted by Mirwaldt et al. (*9*)] at the entrance to the active site (Figure 3). The refined structures of each mutant DHDPS show that this helix is not reorganized and that the side chains at position 138 are oriented similarly to Arg138 of the wild type.

In the DHDPS-R138H structure, the histidine is oriented such that a hydrogen bond links the δ-nitrogen of the imidazole ring to the backbone oxygen of Tyr107. A similar link is also formed with arginine in the wild type. This explains the poor affinity of DHDPS-R138H for the carboxyl of (*S*)-ASA, as the ϵ-nitrogen of the histidine is likely to be unprotonated and unable to bind the carboxyl group. Such problems would be absent in DHDPS-R138A. Interestingly, even though no such connection is seen in the DHDPS-R138A enzyme, Tyr107 is still in a strained conformation in the Ramachandran plot. Thus, it would seem that the orientation of Tyr107 is due to the hydrophobic stacking with Tyr106 and Arg138 and the connections within the proton relay.

Of more importance were changes in the other active site residues when compared with the wild-type structure (Figure 6). Lysine 161 and Tyr133 held the same orientation

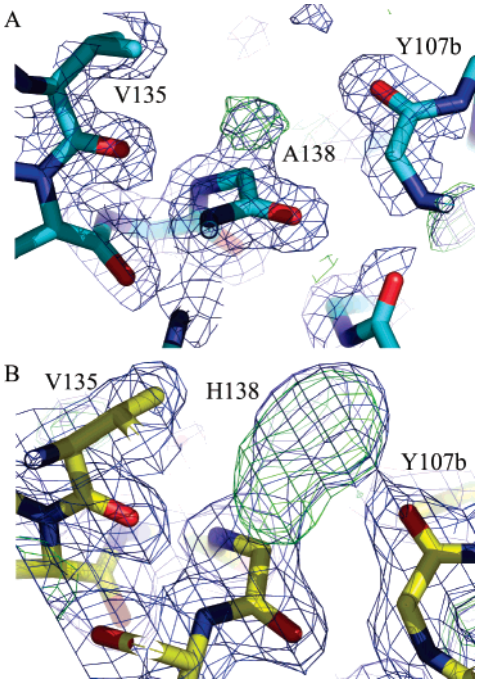

FIGURE 5: Difference map ("omit" map; $2F_o - F_c$ contoured to 1σ, blue; $F_o - F_c$, contoured to 3σ, green) of the mutations at position 138. (A) DHDPS-R138A (cyan). (B) DHDPS-R138H (yellow).

compared to the wild type; however, as evident from the high *B* values for the side chain atoms of Thr44, in the DHDPS-R138A mutant compared to the wild type, this residue appeared to occupy a number of conformations (Figure 7). This is backed up by the presence of extra water molecules in the DHDPS-R138A structure positioned near Thr44 (2.9 Å), which is not seen in the wild-type structure. Different conformations could allow room for water to bind, forming alternate bonding patterns. The apparent flexibility was more pronounced with DHDPS-R138A, where Tyr133 and Tyr107 from subunit B also showed increased *B* values compared to the wild type, presumably because histidine supplies some rigidity that alanine does not. The mean *B* value for DHDPS-R138A (20.6 $Å^2$) was similar to that of the wild type (19.9 $Å^2$). As previously shown, mutation of Thr44 to valine, with concomitant breakage of the proton relay, attenuates catalytic activity (*11*). Also, the distances within the hydrogen-bonding network for both mutations are noticeably lengthened (Table 3). Thus, the lower activity of the DHDPS Arg138 mutants could be attributed to the disruption of this hydrogen-bonding network. Additionally, in both mutant structures, Tyr107, which interacts directly

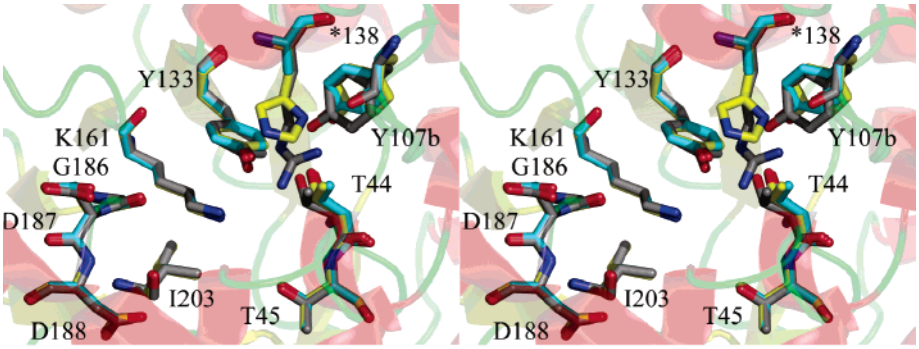

FIGURE 6: Stereoview showing overlays of the active sites of wild-type (black) and mutant DHDPS structures. The rmsd for each mutant dimer in the asymmetric unit with respect to the wild-type dimer was 0.18 and 0.19 Å for DHDPS-R138A and DHDPS-R138H, respectively. Residues from DHDPS-R138A are colored cyan, and those from DHDPS-R138H are colored yellow.

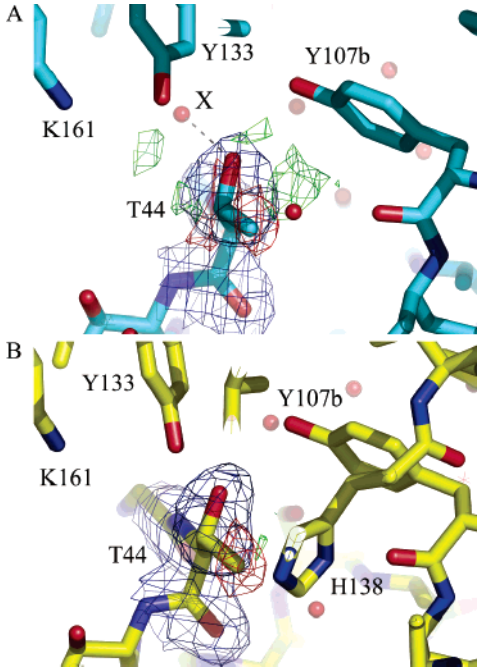

FIGURE 7: Electron density ($2F_o - F_c$, 1σ, blue; $F_o - F_c$, -3σ, red; 3σ, green) surrounding Thr44 in the active site of DHDPS-R138A (A) and DHDPS-R138H (B). The dashed line connects the hydroxyl of Thr44 to a water (X) not seen in other structures (2.91 Å).

Table 3: Comparison of Key Atomic Distances within the Active Site for the Wild-Type and Arginine Mutants of DHDPS

		protein distances (Å)		
		wild type	DHDPS-R138A	DHDPS-R138H
OH Y133	N^{ϵ} K161	2.9	3.5	3.7
OH Y133	OH T44	2.7	3.5	3.1
OH T44	OH Y107	2.7	3.0	3.1
OH Y133	OH Y107	3.7	4.3	4.6
OH Y133	H_2O A	2.6		
H_2O A	N^{ϵ} R138	3.2		
N^{ϵ} K161	=O G186	4.4	5.3	5.3
N^{ϵ} K161	=O I203	5.2	3.7	4.4

with Arg138 in the wild-type enzyme, held a quite different orientation.

Together, this suggests that, apart from binding (*S*)-ASA, Arg138 may also be critical in stabilizing the juxtaposition of Thr44, Tyr133, and Tyr107, perhaps by buttressing these residues via hydrophobic interactions: in the native structure, the β- and δ-carbons of Arg138 are close (~4 Å) to the ring carbons of Tyr107. In addition, a water molecule bridges Arg138_Nϵ to Tyr133_OH in the wild type (*14*). This water is absent in both Arg138 mutants. Taken together, this implies that the binding of (*S*)-ASA, and presumably movement of Arg138, may be a way for the enzyme to modulate the catalytic triad. That is, the pK_a of Tyr133 and its ability to act as a general acid/base could be altered either upon the binding of (*S*)-ASA or, perhaps, during the cyclization step, where movements in Arg138 are presumed to occur (*5*).

(c) (S)-Lysine Inhibition. It is known that (*S*)-lysine inhibits the reaction catalyzed by DHDPS, and others have previously identified the binding site. The precise mechanism by which (*S*)-lysine exerts regulatory control over DHDPS is unclear, although kinetic and structural studies support the proposal that (*S*)-lysine is an allosteric inhibitor (*1*, *5*, *7*, *14*, *28*−*30*).

Others have reported that Arg138 may be important in (*S*)-lysine inhibition (*5*). As such, our mutagenic study was ideal to test this hypothesis. Both DHDPS-R138A and DHDPS-R138H showed similar sensitivity to (*S*)-lysine inhibition when compared to the wild type: for all enzymes, including the wild type, we observed 50% inhibition at 0.2 mM (*S*)-lysine concentration. However, although still a partial inhibitor, both DHDPS-R138A and DHDPS-R138H showed a minimum of 35% activity, even at 10 mM (*S*)-lysine concentrations, compared to the wild type, which was 8% active at this (*S*)-lysine concentration. This may be a result of the changes seen in the flexibility of the triad mutants. The reasons for this altered inhibition pattern are difficult to determine, but we may be further enlightened by the future determination of DHDPS-R138A and DHDPS-R138H with complexed (*S*)-lysine.

Structurally, the allosteric (*S*)-lysine binding site of the mutants is very similar to that of the wild type. This was expected as the (*S*)-lysine binding pocket was not altered by mutagenesis. However, the orientation of the Tyr107 side chain is more similar to the wild type with bound (*S*)-lysine than to the unbound wild-type structure (Figure 8). The phenyl ring is twisted in each mutant by approximately 40° with respect to the wild type. In contrast, for the wild type with bound (*S*)-lysine, the ring is twisted by only 20° (*14*). This is perhaps due to the loss of the hydrophobic stacking between the side chains of Arg138, Tyr107, and Tyr106. That Tyr107 is twisted as in the (*S*)-lysine bound wild type draws into question the role of this movement in the inhibition mechanism.

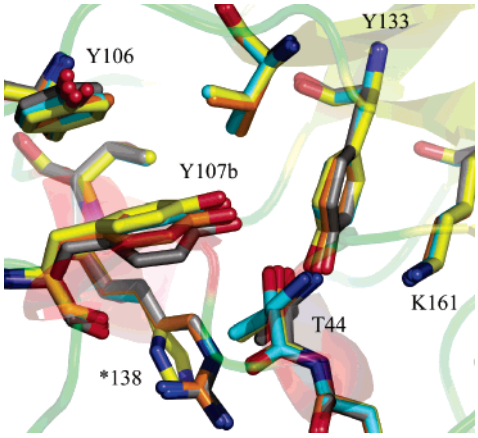

FIGURE 8: Overlay of Tyr107 for the wild-type (gray), wild-type with bound (*S*)-lysine (orange), and both mutations, DHDPS-R138A (cyan) and DHDPS-R138H (yellow).

Taken with our previous structural data (*14*), which found no change in the rigidity of Arg138 upon (*S*)-lysine binding, it is clear that Arg138 does not play a critical role in (*S*)-lysine inhibition. The structural evidence here suggests that the altered pattern of inhibition may be due to changes in the proton relay.

CONCLUSION

This work confirms the hypothesis that arginine 138, which sits on the α5′-helix, is essential for catalysis of (*S*)-ASA and pyruvate to form dihydrodipicolinate by DHDPS. Its likely role is to bind the second substrate, (*S*)-ASA, but, as we have suggested here, it appears that Arg138 may also be important for the stabilization of the proton relay, a motif previously shown to be required for catalysis. Additionally, the role of Arg138 in (*S*)-lysine inhibition was probed, and it was concluded that this residue is not essential in the inhibition mechanism.

ACKNOWLEDGMENT

The authors acknowledge Mike Griffin, Laurence Antonio (University of Canterbury), and especially Antonia Miller (Case Western Reserve University) for critical discussion, along with Sigurd Wilbanks (University of Otago) for help with the CD work. We thank Jackie Healy for unflinching technical support.

REFERENCES

1. Yugari, Y., and Gilvarg, C. (1965) The condensation step in diaminopimelate synthesis, *J. Biol. Chem. 240*, 4710−4716.
2. Coulter, C. V., Gerrard, J. A., Kraunsoe, J. A. E., and Pratt, A. J. (1999) *Escherichia coli* dihydrodipicolinate synthase and dihydrodipicolinate reductase: kinetic and inhibition studies of two putative herbicide targets, *Pestic. Sci. 55*, 887−895.
3. Hutton, C. A., Southwood, T. J., and Turner, J. J. (2003) Inhibitors of lysine biosynthesis as antibacterial agents, *Mini Rev. Med. Chem. 3*, 115−127.
4. Miflin, B. J., Napier, J., and Shewry, P. R. (1999) Improving plant product quality, *Nat. Biotechnol. 17*, 13−14.
5. Blickling, S., Renner, C., Laber, B., Pohlenz, H.-D., Holak, T. A., and Huber, R. (1997) Reaction mechanism of *Escherichia coli* dihydrodipicolinate synthase investigated by X-ray crystallography and NMR spectroscopy, *Biochemistry 36*, 24−33.
6. Shedlarski, J. G., and Gilvarg, C. (1970) The pyruvate-aspartic semialdehyde condensing enzyme of *Escherichia coli*, *J. Biol. Chem. 245*, 1362−1373.
7. Laber, B., Gomis-Rüth, F.-X., Romão, M. J., and Huber, R. (1992) *Escherichia coli* dihydrodipicolinate synthase. Identification of the active site and crystallization, *Biochem. J. 288*, 691−695.
8. Borthwick, E. B., Connel, S. J., Tudor, D. W., Robins, D. J., Shneier, A., Abell, C., and Coggins, J. R. (1995) *Escherichia coli* dihydrodipicolinate synthase: characterisation of the imine intermediate and the product of bromopyruvate treatment by electrospray mass spectrometry, *Biochem. J. 305*, 521−524.
9. Mirwaldt, C., Korndorfer, I., and Huber, R. (1995) The crystal structure of dihydrodipicolinate synthase from *Escherichia coli* at 2.5 Å resolution, *J. Mol. Biol. 246*, 227−239.
10. Lawrence, M. C., Barbosa, J. A. R. G., Smith, B. J., Hall, N. E., Pilling, P. A., Ooi, H. C., and Marcuccio, S. M. (1997) Structure and mechanism of a sub-family of enzymes related to *N*-acetylneuraminate lyase, *J. Mol. Biol. 266*, 381−399.
11. Dobson, R. C. J., Valegård, K., and Gerrard, J. A. (2004) The crystal structure of three site-directed mutants of *Escherichia coli* dihydrodipicolinate synthase: further evidence for a catalytic triad, *J. Mol. Biol. 338*, 329−339.
12. Joerger, A. C., Mayer, S., and Fersht, A. (2003) Mimicking natural evolution *in vitro*: an *N*-acetylneuraminate lyase mutant with an increased dihydrodipicolinate synthase activity, *Proc. Natl. Acad. Sci. U.S.A 100*, 5694−5699.
13. Guillen Schlippe, Y. V., and Hedstrom, L. (2005) A twisted base? The role of arginine in enzyme-catalyzed proton abstractions, *Arch. Biochem. Biophys. 433*, 266−278.
14. Dobson, R. C. J., Griffin, M., Jameson, G. B., and Gerrard, J. A. (2005) The crystal structures of native and (*S*)-lysine-bound dihydrodipicolinate synthase from *Escherichia coli* with improved resolution show new features of biological significance, *Acta Crystallogr. D 61* (Part 8), 1116−1124.
15. Bradford, M. M. (1976) A rapid and sensitive method for the quantitation of microgram quantities of protein utilizing the principle of protein-dye binding, *Anal. Biochem. 72*, 248.
16. Roberts, S. J., Morris, J. C., Dobson, R. C. J., and Gerrard, J. A. (2003) The preparation of (*S*)-aspartate semi-aldehyde appropriate for use in biochemical studies, *Bioorg. Med. Chem. Lett. 13*, 265−267.
17. Selwyn, M. J. (1965) A simple test for the inactivation of an enzyme during assay, *Biochim. Biophys. Acta 105*, 193−195.
18. Cornish-Bowden, A. (1999) *Fundamentals of enzyme kinetics*, 2nd ed., Portland Press Ltd., London.
19. Pflugrath, J. W. (1999) The finer things in X-ray diffraction data collection, *Acta Crystallogr. D55*, 1718−1725.
20. Navaza, J., and Saludjian, P. (1997) AMoRe: An automated molecular replacement program package, *Methods Enzymol. 276*, 581−594.
21. CCP4 (1994) The CCP4 suite: programs for protein crystallography, *Acta Crystallogr. D50*, 760−763.
22. Jones, T., and Kjeldgaard, M. (1997) Electron density map interpretation, *Methods Enzymol. 277*, 173−208.
23. Lamzin, V. S., and Wilson, K. S. (1997) Automated refinement for protein crystallography, *Methods Enzymol. 277*, 269−305.
24. Laskowski, R. A., MacArthur, M. W., Moss, D. S., and Thornton, J. M. (1993) PROCHECK: A program to check the stereochemical quality of protein structures, *J. Appl. Crystallogr. 26*, 283−291.
25. DeLano, W. L. (2002) DeLano Scientific, San Carlos, CA (http://www.pymol.org).
26. Ramachandran, G. N., and Sasisekharan, V. (1968) Conformation of polypeptides and proteins, *Adv. Protein Chem. 23*, 283−437.
27. Rose, G. D., Gierasch, L. M., and Smith, J. A. (1985) Turns in peptides and proteins, *Adv. Protein Chem. 37*, 1−109.
28. Stahly, D. P. (1969) Dihydrodipicolinate synthase of *Bacillus licheniformis*, *Biochim. Biophys. Acta 191*, 439−451.
29. Kumpaisal, R., Hashimoto, T., and Yamada, Y. (1989) Inactivation of wheat dihydrodipicolinate synthase by 3-bromopyruvate, *Agric. Biol. Chem. 53*, 355−359.
30. Blickling, S., Beisel, H.-G., Bozic, D., Knablein, J., Laber, B., and Huber, R. (1997) Structure of dihydrodipicolinate synthase of *Nicotiana sylvestris* reveals novel quaternary structure, *J. Mol. Biol. 274*, 608−621.

BI051281W